

Comparison Between Pseudospectral and Discrete Geometric Methods for Modeling Quantization Effects in Nanoscale Electron Devices

Dimitri Breda¹, David Esseni², Alan Paussa², Ruben Specogna², Francesco Trevisan², and Rossana Vermiglio¹

¹Dip. di Matematica e Informatica, Università di Udine, Via delle Scienze 208, I-33100, Italy

²Dip. di Ingegneria Elettrica, Gestionale e Meccanica, Università di Udine, Via delle Scienze 208, I-33100, Italy

This paper aims at comparing the pseudospectral method and discrete geometric approach for modeling quantization effects in nanoscale devices. To this purpose, we implemented a simulation tool, based on both methods, to solve a self-consistent Schrödinger–Poisson coupled problem for a 2-D electron carrier confinement according to the effective mass approximation model (suitable for FinFETs and nanowire FETs).

Index Terms—Discrete geometric approach (DGA), pseudospectral method, Schrödinger–Poisson problem.

I. INTRODUCTION

THE success of the metal–oxide semiconductor (MOS) technology over the last 30 years has been determined by its scaling capability. These days, the silicon technology is approaching the physical limits of the traditional bulk MOS devices; therefore, new device architectures, such as silicon (Si) nanowire field-effect transistors (FETs) and fin-shaped FETs (FinFETs) could represent a valid alternative to conventional bulk planar metal–oxide semiconductor field-effect transistors (MOSFETs) [1]. Thus, an accurate and yet computationally efficient description of the carrier quantization in these devices is an important modeling target. In the electron device community, the numerical modeling of such a problem is frequently tackled by solving a coupled Schrödinger–Poisson problem, using finite-difference (FD) or finite-elements (FE) methods. The simulation of arbitrarily shaped domains, such as those like real electron devices, is problematic with FD methods; on the contrary, FE methods provide an accurate geometric representation but lead to a discrete counterpart of the Schrödinger problem in terms of a computationally heavy generalized eigenvalue problem.

The aim of this paper is to explore more efficient discretization approaches with respect to FD and FE, such as Pseudospectral methods (PS) [2], [3] and the discrete geometric (DG) approach [4], [5] for self-consistent solution of the Schrödinger–Poisson coupled problem in the case of a 2-D carrier confinement, relevant for nanowire FETs and FinFETs. The PS and DG methods are here benchmarked in terms of geometric modelling capability, by inspecting their accuracy in terms of not only sub-band energies but also of electron concentration distributions.

II. QUANTIZATION IN NANODEVICES

The geometry of interest for a cylindrical nanowire FET is shown in Fig. 1(a). The quantization problem occurs on a bidimensional domain $D = D_{ch} \cup D_{ox}$ on a plane (y, z) normal to the transport direction x , where D_{ch} and D_{ox} denote the channel and oxide domains, respectively [see Fig. 1(b)]; the surrounding gate electrode is modeled as an equipotential domain. In order

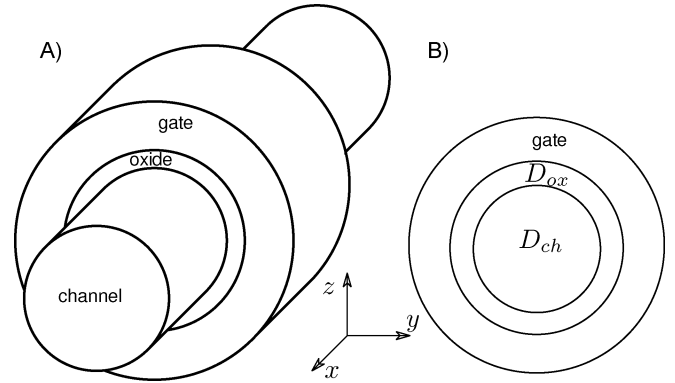


Fig. 1. On the left: device coordinate system (x, y, z) for a cylindrical nanowire FET. On the right: device cross section normal to the transport direction x , where the domain of interest $D = D_{ch} \cup D_{ox}$ is depicted.

to compute the electron density in narrow nanowires and FinFETs, the effective mass approximation (EMA) model is typically adopted to describe the quantization phenomena in D [6]; this leads to the following 2-D Schrödinger equation in D

$$-\text{div } q_\nu(\mathbf{r}) \text{grad } \psi_{\nu,j}(\mathbf{r}) = \lambda_{\nu,j} \psi_{\nu,j}(\mathbf{r}) - u(\mathbf{r}) \psi_{\nu,j}(\mathbf{r}) \quad (1)$$

where ν is the valley¹ index, \mathbf{r} is the position vector of a point $\mathbf{r} = (y, z) \in D$; $\psi_{\nu,j}(\mathbf{r})$ denotes the wave function corresponding to the j th eigenvalue $\lambda_{\nu,j}$; and $q_\nu(\mathbf{r})$ is a double tensor, whose Cartesian components in D are the inverse of effective masses for each valley index ν . Finally, the potential energy $u(\mathbf{r})$ of an electron can be expressed as

$$u(\mathbf{r}) = -e\phi(\mathbf{r}) - \chi(\mathbf{r}) \quad (2)$$

where $\phi(\mathbf{r})$ is the electric scalar potential describing the electrostatic behavior of the nanodevice, e is the absolute value of electron charge, and $\chi(\mathbf{r})$ is the prescribed medium-dependent energy affinity of the electron in D . The interface condition in D and boundary conditions on ∂D must be added to (1), in order to well pose the problem.

The electrostatic behavior of nanodevices can be modeled by coupling to the Schrödinger problem (1) a Poisson problem for the electric scalar potential $\phi(\mathbf{r})$

$$-\text{div } \epsilon(\mathbf{r}) \text{grad } \phi(\mathbf{r}) = -e(N_A^-(\mathbf{r}) + n(\mathbf{r})), \quad \mathbf{r} \in D \quad (3)$$

where $\epsilon(\mathbf{r})$ denotes the medium permittivity double tensor; $N_A^-(\mathbf{r})$ denotes the concentration of ionized acceptor atoms,

¹A valley denotes a conduction-band energy minimum.

Manuscript received June 27, 2011; revised October 11, 2011; accepted October 24, 2011. Date of current version January 25, 2012. Corresponding author: F. Trevisan (e-mail: trevisan@uniud.it).

Color versions of one or more of the figures in this paper are available online at <http://ieeexplore.ieee.org>.

Digital Object Identifier 10.1109/TMAG.2011.2174142

that is null in D_{ox} ; and $n(\mathbf{r})$ denotes electrons concentration in the conduction band. Again, boundary and interface conditions must be added to close the Poisson problem (3).

The coupling between Schrödinger (1) and Poisson (3) problems is two fold. On the one hand, the electric scalar potential $\phi(\mathbf{r})$ determines potential energy $u(\mathbf{r})$ in (2). On the other hand, concentration $n(\mathbf{r})$ of electrons in the conduction band in (3) is given by

$$n(\mathbf{r}) = \sum_{\nu} \sum_j N_{\nu,j} |\psi_{\nu,j}(\mathbf{r})|^2$$

where $N_{\nu,j}$ is a known prescribed function of eigenvalue $\lambda_{\nu,j}$ [7].

III. PSEUDOSPECTRAL METHOD

A first approach to discretize the Schrödinger (1)–Poisson (3) coupled problem is based on the pseudospectral method [2], [8]. The method approximates the unknown function of a differential problem or of an eigenvalue problem by using algebraic or trigonometric polynomials. If the unknown function is sufficiently smooth, the PS method leads to an extremely fast decrease of the approximating error with respect to the degree of the interpolating polynomial N . In particular, the resulting error decays exponentially with N like $O(N^{-p})$ if the function is of class C^p , $p \geq 1$, or even like $O(c^N)$ with $c \in (0, 1)$ if it is analytic. This behavior, known as *spectral accuracy*, results in extremely efficient and fast solvers for differential eigenvalue problems, such as the Schrödinger's Problem (1).

The basics of the PS method are hereafter recalled for a 2-D Cartesian domain, where the unknown function $f(y, z)$, defined in the square $(y, z) \in [0, L_y] \times [0, L_z]$, is approximated by

$$f(y, z) \approx \sum_{j=0}^N \sum_{k=0}^M \ell_{y,j}(y) \ell_{z,k}(z) f(y_j, z_k) \quad (4)$$

where $\ell_{y,j}(y)$ and $\ell_{z,k}(z)$ are N and M -degree Lagrange basis polynomials in the y and z directions, respectively. Since the y and z dependence of $f(y, z)$ in (4) is separately given by $\ell_{y,j}(y)$ and $\ell_{z,k}(z)$, the matrix representative of a partial differential equation can be expressed in terms of differentiation matrices with respect to y and z . As an example, if the discretization points are sorted according to the lexicographical order, so that the column vector $\mathbf{f}_{N,M}$ of the unknown function values reads [8]

$$\mathbf{f}_{N,M} = (f_{0,0} \dots f_{0,M}, f_{1,0} \dots f_{1,M} \dots f_{N,1} \dots f_{N,M})^T \quad (5)$$

then the differentiation matrix $\mathbf{D}_{NM}^{(2)}$ for the second derivative $\partial^2 f(y, z) / \partial y \partial z$ reads

$$\mathbf{D}_{NM}^{(2)} = \mathbf{D}_N^{(1)} \otimes \mathbf{D}_M^{(1)} \quad (6)$$

where the \otimes sign denotes the Kronecker product [8], and $\mathbf{D}_N \in \mathbb{R}^{(1+N) \times (1+N)}$ is the so-called *differentiation matrix*. The entries of \mathbf{D}_N can be expressed as

$$[\mathbf{D}_N]_{ij} = \ell'_{y,j}(y_i), \quad i, j = 0, \dots, N \quad (7)$$

and (7) shows that the differentiation matrices are dense for the PS discretization scheme.

For the circular domain considered in this paper (see Fig. 1), it is convenient to use polar rather than Cartesian coordinates, so that the unknown function has been approximated by using a combination of Chebyshev and Fourier expansions [2]. The transformation to polar coordinates leads to a singularity at $\mathbf{r} =$

0. To overcome this difficulty, we followed the so-called *diameter approach* described in [8].

The basic idea behind the PS method of substituting the unknown function $f(y, z)$ with an interpolating polynomial can also be used to approximate any definite integral of $f(y, z)$ with the integral of the polynomial (Clenshaw–Curtis formula) [8]. This is useful because the same vector $\mathbf{f}_{N,M}$ can thus be employed to calculate different quantities.

In order to preserve all of the advantages of the PS approach for problems with noncontinuous parameters, it is necessary to revisit the method under a piecewise point of view, where the appropriate continuity conditions at the boundaries between different subdomains must be enforced.

IV. DISCRETE GEOMETRIC APPROACH

A second methodology to discretize the Schrödinger (1)–Poisson (3) coupled problem puts the spotlight on the geometrical structure behind a physical theory [5], it is often referred to as the DGA. We will focus here on the discretization of the Schrödinger problem (1), since the discretization of the Poisson problem (3) in electrostatics according to DG is well established [9].

Now, we will reformulate in a slightly different way the left-hand side of (1), in terms of the following relations:

$$-\text{grad } \psi_{\nu,j}(\mathbf{r}) = \mathbf{a}(\mathbf{r}) \quad (8)$$

$$\mathbf{q}_{\nu}(\mathbf{r}) \mathbf{a}(\mathbf{r}) = \mathbf{b}(\mathbf{r}) \quad (9)$$

$$\text{div } \mathbf{b}(\mathbf{r}) = \gamma(\mathbf{r}) \quad (10)$$

where we introduced the vector fields² $\mathbf{a}(\mathbf{r})$, $\mathbf{b}(\mathbf{r})$, and the scalar field $\gamma(\mathbf{r})$, respectively; due to the plane (y, z) symmetry of the problem, the vector and scalar fields introduced before are invariant for any plane normal to the x axis. Besides, we rewrite the right-hand side of (1) as

$$(\lambda_{\nu,j} - u(\mathbf{r})) \psi_{\nu,j}(\mathbf{r}) = \gamma(\mathbf{r}). \quad (11)$$

Of course, (8)–(10) and (11) are equivalent to (1). We note that (9) and (11) play the role of constitutive relations between a pair of vector and scalar fields, respectively, with $\mathbf{q}(\mathbf{r})$ and $\lambda_{\nu,j} - u(\mathbf{r})$ being the medium characteristics.

A. Domain Discretization

We introduce in D the same discretization for the Schrödinger and Poisson problems. The discretization consists of a primal *simplicial* cell complex $\mathcal{K} = \{\mathcal{N}, \mathcal{E}, \mathcal{F}, \mathcal{V}\}$, whose oriented geometrical elements are nodes $n_i \in \mathcal{N}$, edges $e_j \in \mathcal{E}$, faces $f_h \in \mathcal{F}$, and volumes $v_k \in \mathcal{V}$ (triangular prisms), [5] (Fig. 2). The cardinality of each set $\mathcal{N}, \mathcal{E}, \mathcal{F}, \mathcal{V}$ is denoted by N, E, F , and V , respectively. From the primal cell complex \mathcal{K} , we can construct a *barycentric* dual complex $\tilde{\mathcal{K}} = \{\tilde{\mathcal{V}}, \tilde{\mathcal{F}}, \tilde{\mathcal{E}}, \tilde{\mathcal{N}}\}$, whose oriented geometrical elements are dual nodes $\tilde{n}_k \in \tilde{\mathcal{N}}$, dual edges $\tilde{e}_h \in \tilde{\mathcal{E}}$, dual faces $\tilde{f}_j \in \tilde{\mathcal{F}}$, and dual volumes $\tilde{v}_i \in \tilde{\mathcal{V}}$. Finally, we need the incidence matrix \mathbf{G} of dimension $E \times N$ of incidence numbers G_{ji} between orientations of pairs (e_j, n_i) and $-\mathbf{G}^T$ describing the incidences between the orientations of pairs $(\tilde{v}_i, \tilde{f}_j)$.

B. Integral Variables and Their Association with the Elements of $\mathcal{K}, \tilde{\mathcal{K}}$

We introduce the array Ψ of dimension N , whose i th entry $\Psi_i = \psi_{\nu,j}(\mathbf{r}_{n_i})$ is the value $\psi_{\nu,j}(\mathbf{r}_{n_i})$ assumed at the posi-

²A vector is always denoted in roman type.

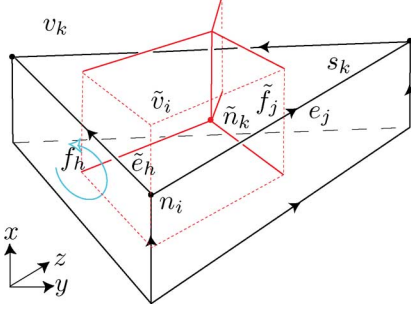


Fig. 2. Oriented geometric elements of the primal complex \mathcal{K} and of the dual complex $\bar{\mathcal{K}}$ restricted, for clarity, to a single triangular prism v_k which is in a one-to-one correspondence with the triangular surface s_k .

tion r_{n_i} of the node n_i , with $i = 1, \dots, N$. The circulation $A_j = \int_{e_j} \mathbf{a}(\mathbf{r}) \cdot d\mathbf{l}$ of the vector $\mathbf{a}(\mathbf{r})$ along a primal edge e_j is associated with primal edges, with $j = 1, \dots, E$; the array \mathbf{A} they form has dimension E . Similarly, but at a different geometric level, the flux $B_j = \int_{\tilde{f}_j} \mathbf{b}(\mathbf{r}) \cdot d\mathbf{s}$ of the vector $\mathbf{b}(\mathbf{r})$ across a dual face \tilde{f}_j is associated with dual faces, with $j = 1, \dots, E$ and the array \mathbf{B} they form having dimension E . Finally, we introduce the integral quantity $\Gamma_i = \int_{\tilde{v}_i} \gamma(\mathbf{r}) d\mathbf{v}$, associated with a dual volume \tilde{v}_i , with $i = 1, \dots, N$, and we denote with $\bar{\Gamma}$ the corresponding array that they form, of dimension N . The arrays Ψ , \mathbf{A} , \mathbf{B} , and $\bar{\Gamma}$ of integral variables are often referred to as degrees of freedom (DoF).

C. Balance Equations and Constitutive Relations

Now, according to algebraic topology [5], we can straightforwardly construct *exact* discrete counterparts of (8) and (10), respectively, in terms of the introduced DoF arrays with respect to the topology of the pair of cell complexes \mathcal{K} , $\bar{\mathcal{K}}$ and we obtain

$$-\mathbf{G}\Psi = \mathbf{A} \quad (\text{a}), \quad -\mathbf{G}^T\mathbf{B} = \bar{\Gamma} \quad (\text{b}). \quad (12)$$

These relations are independent of the media and metric of the pair of cell complexes in D .

A crucial point of the discretisation process is the computation of *approximated* discrete counterparts of the constitutive relations (9) and (11), which can be written, respectively, as

$$\mathbf{M}\mathbf{A} = \mathbf{B} \quad (\text{a}), \quad \mathbf{N}\Psi = \bar{\Gamma} \quad (\text{b}) \quad (13)$$

where \mathbf{M} and \mathbf{N} are square matrices of dimension E and N , respectively, depending on metric and media properties of the pair of cell complexes [4].

D. Discrete Formulated Schrödinger Problem

By substituting (12b) and (13a) for \mathbf{B} , (12a) for \mathbf{A} and (13b) for $\bar{\Gamma}$, a discrete counterpart of (1) becomes

$$\mathbf{G}^T\mathbf{M}\mathbf{G}\Psi = \mathbf{N}\Psi. \quad (14)$$

The global stiffness matrix $\mathbf{G}^T\mathbf{M}\mathbf{G}$ is obtained by assembling the contributions from the local stiffness matrices of each triangle s_k , with $k = 1, \dots, V$. The entry $(\mathbf{G}^T\mathbf{M}\mathbf{G})_{lm}^k$ of a local symmetric stiffness matrix can be expressed efficiently [4] in a pure geometric way for the triangle s_k as

$$(\mathbf{G}^T\mathbf{M}\mathbf{G})_{lm}^k = \frac{1}{4|s_k|} \mathbf{f}_l \cdot \mathbf{q}_\nu \mathbf{f}_m, \quad l, m = 1, \dots, 3 \quad (15)$$

where $|s_k|$ is the area of s_k , and \mathbf{f}_l is the area vector³ associated with the lateral face f_l of v_k .

Similarly, the global matrix \mathbf{N} is obtained by assembling the local matrix \mathbf{N}^k contributions from each triangular element s_k , with $k = 1, \dots, V$; according to [4], \mathbf{N}^k can be written as the sum of a pair of local *diagonal* matrices

$$(\mathbf{N})^k = \lambda_{\nu,j} (\mathbf{N}')^k - (\mathbf{N}_u)^k \quad (16)$$

whose entries are $\delta_{lm}(|s_k|/3)$, $\delta_{lm}(|s_k|/3)u^k$, respectively, where u^k is the uniform value $u(\mathbf{r})$ assumes in v_k .

From (14), we obtain the final global generalized eigenvalue problem

$$(\mathbf{G}^T\mathbf{M}\mathbf{G} + \mathbf{N}_u)\Psi = \lambda_{\nu,j} \mathbf{N}'\Psi \quad (17)$$

where \mathbf{N}_u and \mathbf{N}' are the global diagonal matrices corresponding to the local ones in (16). Since \mathbf{N}' is diagonal and positive definite, then (17) can be easily transformed into a standard one and we may write

$$(\mathbf{N}')^{-1/2}(\mathbf{G}^T\mathbf{M}\mathbf{G} + \mathbf{N}_u)(\mathbf{N}')^{-1/2}\Psi' = \lambda_{\nu,j}\Psi' \quad (18)$$

where we set $\Psi' = (\mathbf{N}')^{1/2}\Psi$.

V. NUMERICAL RESULTS AND DISCUSSION

We solved the coupled problem for a cylindrical nanowire with $d = 10$ nm and a transport orientation along the x direction using the DG and the PS methods. In order to obtain an efficient convergence of the Schrödinger–Poisson iterative loop, both for DG and the PS methods, we employed the so-called nonlinear formulation of the Poisson equation described in [7]. A doping density $N_A = 1 \times 10^{15} \text{ cm}^{-3}$, an equivalent oxide thickness of 0.7 nm, and a gate work function ϕ_m equal to the electron affinity $\chi(\mathbf{r}) = 4.05$ eV of silicon have been considered in the simulations. A gate voltage $V_G = 1$ V is used to specify the Dirichlet boundary conditions on ∂D for the Poisson problem, while $\psi_{\nu,j}(\mathbf{r}) = 0$ for $\mathbf{r} \in \partial D$ is assumed for the Schrödinger problem. The diagonal entries of $\epsilon(\mathbf{r})$ tensor are $3.9\epsilon_0$ for $\mathbf{r} \in D_{ox}$ and $11.7\epsilon_0$ for $\mathbf{r} \in D_{ch}$, with ϵ_0 being the vacuum permittivity. In our problem, tensor $\mathbf{q}_\nu(\mathbf{r})$ is anisotropic with diagonal⁴ entries depending both on the index ν , being proportional to $\hbar^2/(2m_0)$, with $m_0 = 5.6810^{-30} \text{ eVs}^2\text{nm}^{-2}$ the free electron mass. Fig. 3 compares the convergence of the first and second valley minimum eigenvalues for an increasing number of nodes, computed by means of the DG and PS approaches, respectively; moreover, the electron concentration n along the y axis computed with the DG and PS method for an increasing number of nodes is shown in Fig. 4. For completeness, Fig. 5 shows the anisotropic charge density distribution in the cylindrical nanowire on a plane normal to the x transport direction; the computation with the PS or DG methods yields to graphically indistinguishable results.

Even though the PS method ensures spectral accuracy, it is limited to simple shape geometries such as the circular one of the specific device considered here or the rectangular one; moreover, it always yields to full (but smaller) differentiation matrices. On the other hand, the DG approach shows a slower convergence compared with the PS method, being based on an element-wise uniform field approximation; however, DG can handle complicated geometries like those of the real devices. In addition, the proposed DG approach straightforwardly yields

³It is normal to the lateral face f_l of the prism and it points outward v_k ; moreover, due to the plane symmetry, $|\mathbf{f}_l| = |e_l|$ holds.

⁴For the detailed expression of the tensor $\mathbf{q}_\nu(\mathbf{r})$, see [2].

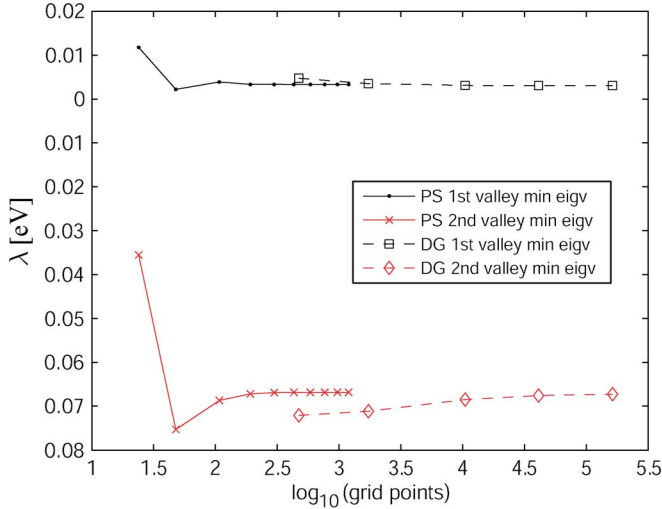


Fig. 3. Convergence of the first and second valley minimum eigenvalues is compared for an increasing number of nodes, computed by means of the DG and PS approaches, respectively.

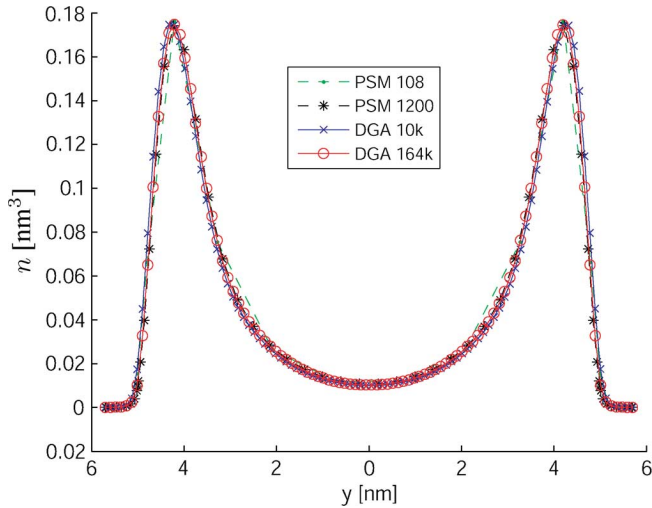


Fig. 4. Electron concentrations n along the y direction, computed with the DG and PS methods for a $d = 10$ -nm cylindrical nanowire.

to a standard eigenvalue problem since the matrix \mathbf{N}' in (17) is diagonal; on the contrary, in finite elements, the matrix corresponding to \mathbf{N}' in (17) is not diagonal, having the same sparsity pattern of the matrix on the left-hand side of (17). This fact makes, by construction, DG computationally more efficient than FE since the memory occupation is about one half. We observe that there is no need to compute the matrix products in (18); it is enough to multiply each nonzero ij entry of the sparse matrix $(\mathbf{G}^T \mathbf{M} \mathbf{G} + \mathbf{N}_u)$ by $(\mathbf{N}')_i^{-1/2} (\mathbf{N}')_j^{-1/2}$ with $i, j = 1, \dots, N$, where $(\mathbf{N}')_i^{-1/2}$ denotes the i th diagonal element of $(\mathbf{N}')^{-1/2}$. Moreover, the generalized eigenvalue problem produced by FE requires solving a linear system at each step of the iterative solution in place of a simple matrix-vector product needed by the standard eigenvalue problem of DG. Finally, the finite-difference method has not been tested deliberately for our specific geometries.

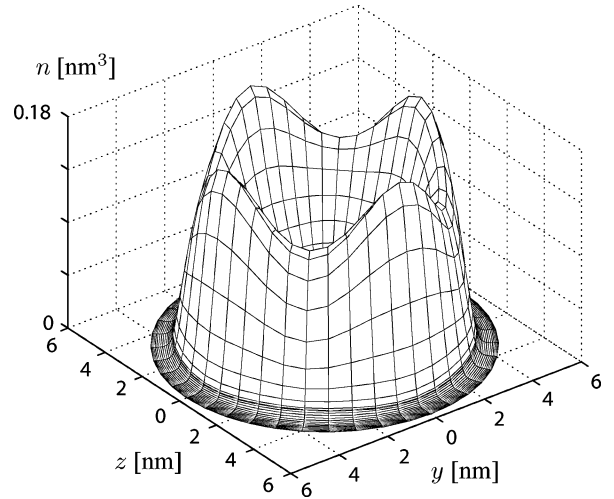


Fig. 5. Electron concentration n in the cylindrical nanowire. The computation with the PS or DG methods yields to graphically indistinguishable results.

VI. CONCLUSION

A comparative analysis confirmed that pseudospectral methods can achieve the spectral accuracy but are mainly suitable for simple geometries. On the contrary, the DGA allowed handling more complex and general 2-D and 3-D geometries. Both techniques yield a discrete counterpart of the Schrödinger problem in the form of a standard matrix eigenvalue problem, instead of a generalized one like in finite elements.

ACKNOWLEDGMENT

This work was supported in part by EU (NANOSIL NoE No. IST-216171) and in part by the ENIAC.JTI-MODERN project. The authors would like to thank Prof. L. Selmi and Prof. P. Palestri for encouraging this joint collaboration.

REFERENCES

- [1] Y. Taur, D. A. Buchanan, W. Chen, D. J. Frank, K. E. Ismail, S.-H. Lo, G. A. Sai-Halasz, R. G. Viswanathan, H. C. Wann, S. J. Wind, and H.-S. Wong, "CMOS scaling into the nanometer regime," *Proc. IEEE*, vol. 85, no. 4, pp. 486–503, Apr. 1997.
- [2] A. Paussa, F. Conzatti, D. Breda, R. Vermiglio, D. Esseni, and P. Palestri, "Pseudospectral methods for the efficient simulation of quantization effects in nanoscale MOS transistors," *IEEE Trans. Electron Devices*, vol. 57, no. 12, pp. 3239–3249, Dec. 2010.
- [3] W. Heinrichs, "Spectral collocation schemes on the unit disc," *J. Comput. Phys.*, vol. 199, no. 1, pp. 66–86, 2004.
- [4] R. Specogna and F. Trevisan, "A discrete geometric approach to solving time independent Schrödinger equation," *J. Comput. Phys.*, vol. 230, pp. 1370–1381, 2011.
- [5] E. Tonti, "Algebraic topology and computational electromagnetism," in *Proc. 4th Int. Workshop Elect. Magn. Fields*, Marseille, France, May 12–15, 1998, pp. 284–294.
- [6] M. Bescond, N. Cavassilas, and M. Lannoo, "Effective-mass approach for n-type semiconductor nanowire MOSFETs arbitrarily oriented," *Nanotechnol.*, vol. 18, no. 25, p. 255201, 2007, (6pp).
- [7] A. Trellakis, A. T. Galick, A. Pacelli, and U. Ravaioli, "Iteration scheme for the solution of the two-dimensional Schrödinger-poisson equations in quantum structures," *J. Appl. Phys.*, vol. 81, no. 12, pp. 7880–7884, 1997.
- [8] L. N. Trefethen, *Spectral Methods in MATLAB*. Philadelphia, PA: SIAM, 2000.
- [9] P. Bettini and F. Trevisan, "Electrostatic analysis for plane problems with finite formulation," *IEEE Trans. Magn.*, vol. 39, no. 3, pp. 1127–1130, May 2003.
- [10] J. Blakemore, "Approximations for fermi-dirac integrals, especially the function used to describe electron density in a semiconductor," *Solid-State Electron.*, vol. 25, no. 11, pp. 1067–1076, 1982.